

# Mechanical Properties and Fire Retardancy of Wood Flour/High-Density Polyethylene Composites Reinforced with Continuous Honeycomb-Like Nano-SiO<sub>2</sub> Network and Fire Retardant

Haiyang Zhou<sup>1,2</sup>, Xiaoyu Wang<sup>3</sup>, Xiaolong Hao<sup>1,2</sup>, Qingwen Wang<sup>1,2,\*</sup> and Rongxian Ou<sup>1,2,\*</sup>

<sup>1</sup>Key Laboratory for Biobased Materials and Energy of Ministry of Education, College of Materials and Energy, South China Agricultural University, Guangzhou, 510642, China

<sup>2</sup>Guangdong Laboratory for Lingnan Modern Agricultural Science and Technology, Guangzhou, 510642, China

<sup>3</sup>College of Arts, South China Agricultural University, Guangzhou, 510642, China

\*Corresponding Authors: Qingwen Wang. Email: qwwang@scau.edu.cn; Rongxian Ou. Email: rongxian\_ou@scau.edu.cn

Received: 22 February 2020; Accepted: 02 April 2020

**Abstract:** The mechanical properties of wood flour/high-density polyethylene composites (WPC) were improved by adding a small amount of nano-SiO<sub>2</sub> to obtain a network-structured WPC with a continuous honeycomb-like nano-SiO<sub>2</sub> network. The wood flour was modified with a fire retardant (a mixture of sodium octabonate and amidine urea phosphate) to improve its fire retardancy. The flexural properties, creep resistance, thermal expansion, and fire retardancy of the WPC were compared to a control (WPC<sub>CTRL</sub>) without nano-SiO<sub>2</sub> or fire retardant. The flexural strength and modulus of the WPC containing only 0.55 wt.% nano-SiO<sub>2</sub> were 6.6% and 9.1% higher than the control, respectively, while the creep strain and thermal expansion rate at 90°C were 33.8% and 13.6% lower, respectively. The cone calorimetry tests revealed that the nano-SiO<sub>2</sub> network physically shielded the WPC, giving it lower heat release and smoke production rates. The thermal expansion was further decreased by incorporating fire retardants into the WPC, which showed the lowest total heat release and total smoke production and the highest mass retention. This study demonstrates a facile procedure for producing WPC with desired performances by forming a continuous honeycomb-like network by adding a small amount of nanoparticles.

**Keywords:** Wood plastic composites; nano-SiO<sub>2</sub>; mechanical properties; creep; fire retardancy

## 1 Introduction

Wood flour/thermoplastic composites (WPC) are environmentally-friendly materials that have been extensively used in building, decorative, and logistics packing materials [1–3]. Nonpolar polyolefins (polyethylene and polypropylene) are used as thermoplastics in WPCs due to their facile processing and forming, low cost, and similar processing temperatures to wood flour. The wood flour originates from wood processing residues, waste wood products, and agricultural and forestry residues. Weak interfaces are formed between the polar wood flour and nonpolar polyolefins due to their surface energy differences,



This work is licensed under a Creative Commons Attribution 4.0 International License, which permits unrestricted use, distribution, and reproduction in any medium, provided the original work is properly cited.

which results in low mechanical strength and creep resistance of the resulting WPC, which limit their applications and shorten their service life [4–6].

Many studies have investigated methods to improve the strength and creep resistance of WPC [7], including increasing interfacial compatibility and adding inorganic nanoparticles. For example, grafting a mixture of polyethylene and polypropylene with maleic anhydride monomers improved the compatibility between grafted polymers and wood flour. The flexural strength and modulus of the resulting WPC increased by 117% and 29%, respectively, while the creep strain was lowered [8]. The incorporation of maleic anhydride-grafted polypropylene into wood fiber/polypropylene composites increased the creep modulus by nearly 28.0% at 60°C [9]. The creep resistance of wood flour/polypropylene composites increased by about 15% and 22.5% after the addition of 1 wt.% nanoclay and transition metal-modified nanoclay, respectively [10]. The flexural strength and modulus of polylactic acid composites after the wood fiber was modified with 3 wt.% organo-montmorillonite increased by 30.7% and 46.8%, respectively [11].

Nano-SiO<sub>2</sub> is a commercially-available inorganic filler that is easy to produce on large scales, low-cost, and easily undergoes surface modification. It has the potential to improve the creep resistance and fire retardancy of WPC [11,12]. The incorporation of 8 wt.% SiO<sub>2</sub> in polyethylene/polypropylene/flax ternary composites significantly reduced the creep strain and improved the relaxation modulus [12]. Adding 14 wt.% nano-SiO<sub>2</sub> to wood flour/polyethylene composites reduced the average heat release rate and total heat release by 30.3% and 12.8%, respectively, while it increased the smoke release [13]. To obtain satisfactory creep resistance and fire retardation, high nano-SiO<sub>2</sub> loadings are required when using traditional processes to directly disperse nano-SiO<sub>2</sub> in WPC [14,15]. This increases the cost and decreases the mechanical properties of WPC due to the agglomeration of nano-SiO<sub>2</sub> [15].

In order to enhance the mechanical properties and creep resistance of WPC, a continuous honeycomb-like nano-SiO<sub>2</sub> network was formed in a WPC using solution mixing, rotary evaporation, and mold pressing. In the network-structured WPC, SiO<sub>2</sub> nanoparticles were distributed only at the boundaries between the WPC pellets instead of uniformly throughout the WPC. Thus, the amount of nano-SiO<sub>2</sub> was significantly reduced. In order to further improve the fire retardancy of the network-structured WPC, wood flour modified with fire retardants (amidine urea phosphate and sodium octaborate tetrahydrate) was used to fabricate WPC. The flexural properties, creep resistance, thermal expansion, and fire retardancy of the resulting WPC were evaluated.

## 2 Experimental

### 2.1 Materials

HDPE pellets with a density of 0.954 g/cm<sup>3</sup> and a melt flow index of 0.9 g/10 min were obtained from Daqing Petrochemical Co., Ltd. (Daqing, China). Wood flour (WF) with a particle size of 40–60 mesh was prepared from poplar wood (*Populus adenopoda* Maxim) in our laboratory. Maleic anhydride-grafted polyethylene (MAPE) pellets with a grafting ratio of 0.9 wt.% and a melt flow index of 1.9 g/10 min were purchased from Sunny New Technology Development Co., Ltd. (Shanghai, China). The lubricant was a mixture of stearic acid and polyethylene wax (1:1 in mass, Adisi Co., Ltd., Nanjing, China). SiO<sub>2</sub> nanoparticles with an average diameter of 10–15 nm (marked as nSiO<sub>2</sub>) were obtained from Meng Tai Hu Industrial Co., Ltd. (Shanghai, China). The fire retardant (FR) was a mixture of guanlyurea phosphate (abbr: GUP; molecular formula: C<sub>2</sub>H<sub>9</sub>N<sub>4</sub>O<sub>5</sub>P; purity: 99.04%; free phosphoric acid content: 0.41%) and sodium octaborate tetrahydrate (abbr: DOT; molecular formula: Na<sub>2</sub>B<sub>8</sub>O<sub>13</sub>·4H<sub>2</sub>O; melting point: 741°C). The mass ratio of GUP-to-DOT was 7:3 and was made in-house. Vinyltrimethoxysilane (abbr: VTS) was purchased from Chi Ye Silicone Co., Ltd. (Shanghai, China). Ethanol solution was obtained from Tianjin Guangfu Co., Ltd. (Tianjin, China).

## 2.2 Experimental

### 2.2.1 Fire Retardant Impregnated Poplar Powder

WF was dried in a vacuum oven at 103°C for 12 h to reach 1–2% moisture content. The dried WF was impregnated in a 9 wt.% aqueous solution of fire retardant through vacuum treatment at  $-0.01$  MPa for 6 h. Then, the impregnated WF was drained on a 100-mesh sieve, followed by vacuum drying at 80°C for 12 h to obtain the modified WF (Fig. 1). The weight gain rate of the modified WF was  $11.25 \pm 1.06\%$ . WF was also treated with distilled water using the same process as the unmodified WF.

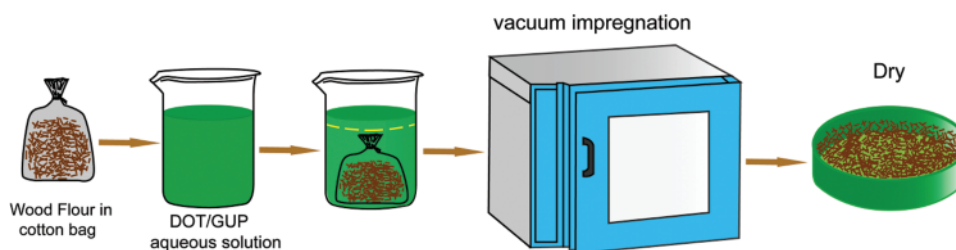


**Figure 1:** Schematic diagram of wood flour impregnated with fire retardant

### 2.2.2 Preparation of WPC

The unmodified WF or modified WF and HDPE, MAPE, and lubricant were compounded for 8 min at ambient temperature using a high-speed mixer (SHR-10A; Tongsha Plastic Machinery Company, Zhangjiagang, China). The mixture was melt-blended through a co-rotating twin-screw extruder (diameter = 40 mm, L/D = 30, SJSH-30, Nanjing Rubber Machinery Corp., Nanjing, China) at a temperature range of 145–165°C. The resulting extrudates were pelletized.

**Preparation of control WPC and fire retardant (FR)-modified WPC:** The obtained pellets were molded into panels (160 mm × 160 mm × 3 mm) using a flat vulcanizing machine (XH-406B; Zhuosheng Machinery Equipment Co., Ltd., Dongguan, China) at 180°C with a pressure of 12 MPa for 3 min after pre-pressing for 15 min. The obtained WPC panels with unmodified WF or modified WF were referred to as WPC<sub>CTRL</sub> and WPC<sub>F</sub>, respectively. The weight ratio of each component in the panels is shown in Tab. 1.

**Table 1:** Weight ratio of each component in WPC panels (wt.%) (WPC<sub>CTRL</sub> = control; WPC<sub>S</sub> = WPC panel with nSiO<sub>2</sub> network; WPC<sub>F</sub> = WPC panel with fire retardant modified wood flour; WPC<sub>SF</sub> = WPC panel with nSiO<sub>2</sub> network and fire retardant modified wood flour)

Sample	nSiO <sub>2</sub>	Fire retardant	Wood flour	HDPE	MAPE	lubricant
WPC <sub>CTRL</sub>	0	0	50	45	3	2
WPC <sub>S</sub>	0.55	0	49.45	45	3	2
WPC <sub>F</sub>	0	5.63	44.37	45	3	2
WPC <sub>SF</sub>	0.75	5.63	43.62	45	3	2

**Preparation of network-structured WPC based on nSiO<sub>2</sub>:** The pellets obtained in Section 2.2.2 were uniformly mixed with nSiO<sub>2</sub> (3 wt.% based on the WPC pellets) using an electric mixer in an ethanol solution. Subsequently, nSiO<sub>2</sub>-coated WPC pellets were obtained after evaporating ethanol. The nSiO<sub>2</sub>-coated pellets were screened through a 30-mesh sieve to remove self-agglomerated nSiO<sub>2</sub>. The WPC panels prepared using the nSiO<sub>2</sub>-coated pellets with unmodified WF and modified WF were marked as

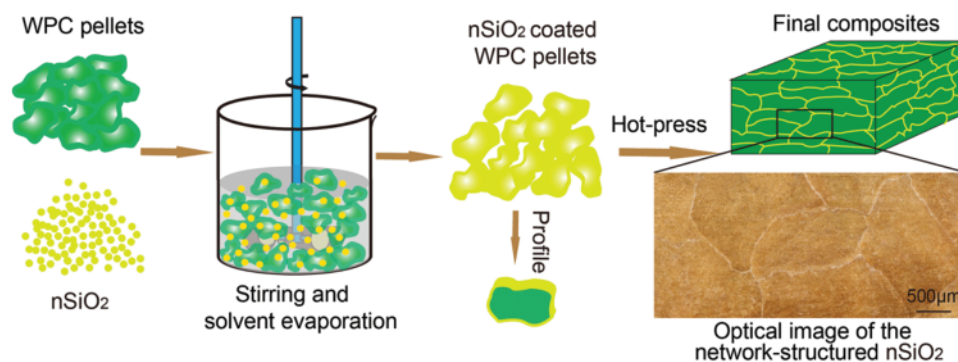


**Figure 2:** Schematic diagram of processing process of the network-structured WPC

WPC<sub>S</sub> and WPC<sub>SF</sub>, respectively. The amounts of nSiO<sub>2</sub> coated on the pellets were calculated and are shown in Tab. 1. In the network-structured WPC panels, nSiO<sub>2</sub> was distributed at the boundary between the WPC pellets (Fig. 2). The optical microscopic image in Fig. 2 shows that nSiO<sub>2</sub> formed a continuous honeycomb-like network in the WPC.

### 2.3 Characterization

The micro-morphologies of the WPC pellets and the cross-sections of the WPC panels were observed using a scanning electron microscope (SEM, FEI QuanTa200, FEI Co., Hillsboro, OR, USA) at an accelerating voltage of 12.5 kV. The WPC pellets and panels were sputter-coated with gold. In addition, the elemental distribution of the surfaces of the WPC pellets was analyzed using energy-dispersive spectrometry (EDS).

The flexural properties of the WPC panel samples (80 mm × 13 mm × 4 mm) were analyzed by a universal mechanical testing machine (CMT5504, MTS Systems Co., Ltd, China) according to ASTM D790-10. Eight replicates were tested for each group.

Creep and relaxation tests of samples (35 mm × 12 mm × 3.5 mm) were performed on a dynamic mechanical analyzer (Q800, TA Instruments Inc., SA). Isothermal (50°C) creep was tested for 50 min under a load of 2 MPa within the elastic deformation regime. Relaxation was tested under a constant strain of 0.1%, and the change in the relaxation modulus was recorded.

Thermal expansion of the specimens measuring 10 mm × 10 mm × 3.5 mm (length × width × thickness) was analyzed along the thickness direction using a thermomechanical analyzer (Q400, TA Instruments Inc., USA). Specimens were heated from room temperature to 100°C at a heating rate of 20 °C/min and then held at 100°C for 3 min to eliminate the thermal history and moisture. A quartz probe was in contact with the specimens under a loaded of 0.05 N. The tests were conducted from −40°C to 90°C at a heating rate of 3°C/min under a nitrogen atmosphere.

The fire retardancy tests of WPC specimens measuring 100 mm × 100 mm × 3.5 mm were conducted using a cone calorimeter (Fire Testing Technology Ltd., East Grinstead, UK) according to ISO 5660-1 at a heat flux of 50 kW/m<sup>2</sup>. The heat release rate (HRR), total heat release (THR), smoke production rate (SPR), total smoke production (TSP), and residual mass were recorded. Two replicates were tested for each group. The residuals after combustion were analyzed by a digital camera and SEM.

## 3 Results and Discussion

### 3.1 Morphological Analysis

The WPC<sub>CTRL</sub> pellets had a rough and uneven surface on which the WF was imbedded in an HDPE matrix (Fig. 3a). The surface morphology of the WPC<sub>F</sub> pellets was similar to that of the WPC<sub>CTRL</sub> pellets

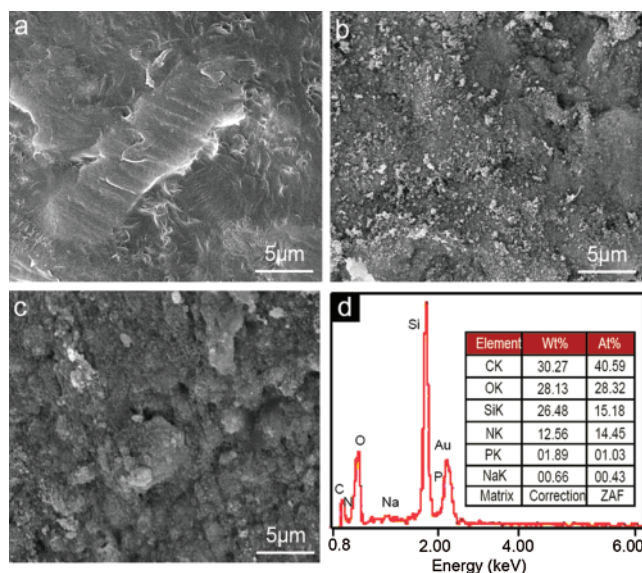


**Figure 3:** SEM micrographs of the surface of the WPC control pellets (a), the WPC pellets coated with nano-SiO<sub>2</sub> (b), and the fire retardant modified WPC pellets coated with nano-SiO<sub>2</sub> (c); EDS corresponding to Fig. 3c (d)

(not shown). The nSiO<sub>2</sub> particle aggregates were visible on the WPC<sub>S</sub> pellets (Fig. 3b). For the WPC<sub>SF</sub> pellets, the nSiO<sub>2</sub> particles and WF were enveloped by a viscous substance (Fig. 3c). The EDS result showed that the viscous substance contained a small amount of N and P (Fig. 3d), indicating that it may be the product of dissolving GUP in ethanol. The viscous substance could facilitate the adhesion of more nSiO<sub>2</sub> particles, as demonstrated by the higher nSiO<sub>2</sub> content on the WPC<sub>SF</sub> pellet surface than on the WPC<sub>S</sub> pellet surface (Tab. 1).

The SEM micrographs of the cross-sections of the flexural-fractured WPC panels are shown in Fig. 4. The HDPE matrix underwent plastic deformation, as shown in the fracture cross-sections of the WPC<sub>CTRL</sub> and WPC<sub>F</sub> (Figs. 4a and 4b). This was a result of the flexural failure loading mode [16]. A continuous nSiO<sub>2</sub>-rich region was observed on the fractured cross-section of WPC<sub>S</sub> (Fig. 4c). This region exhibited brittle fracture compared with the WPC region due to the high nSiO<sub>2</sub> content, and there was no obvious boundary between the WPC pellets after hot-pressing. Furthermore, the high-magnification images of the nSiO<sub>2</sub>-rich region showed a mixture of nSiO<sub>2</sub> and HDPE (Fig. 4d) due to the diffusion of molten HDPE into the nSiO<sub>2</sub> lamella during hot-pressing. Compared with the WPC<sub>S</sub>, the WPC<sub>SF</sub> showed a wider nSiO<sub>2</sub>-rich region on the fractured cross-section (Fig. 4e) due to the higher nSiO<sub>2</sub> content. The nSiO<sub>2</sub>-rich region of WPC<sub>SF</sub> (Fig. 4f) exhibited more ductile fracture behavior compared with WPC<sub>S</sub> (Fig. 4d), possibly because the viscous substance enveloping the nSiO<sub>2</sub> surface reduced the interfacial compatibility between nSiO<sub>2</sub> and HDPE in the nSiO<sub>2</sub>-rich region of WPC<sub>SF</sub>.

### 3.2 Flexural Properties

The flexural strength of WPC<sub>S</sub> (37.3 MPa) was higher than that of WPC<sub>CTRL</sub> (35.0 MPa) due to the formation of a rigid nSiO<sub>2</sub> network (Fig. 5a) which could transfer stress due to its compatibility with the HDPE matrix [17]. Compared with the WPC<sub>CTRL</sub>, the flexural strength of WPC<sub>F</sub> (33.5 MPa) was slightly lower due to the weak interfacial bonding between the fire retardant-impregnated WF and HDPE matrix [18,19]. The flexural strength of WPC<sub>SF</sub> (33.0 MPa) was further decreased compared with that of WPC<sub>F</sub> because the viscous substance weakened the nSiO<sub>2</sub> network.

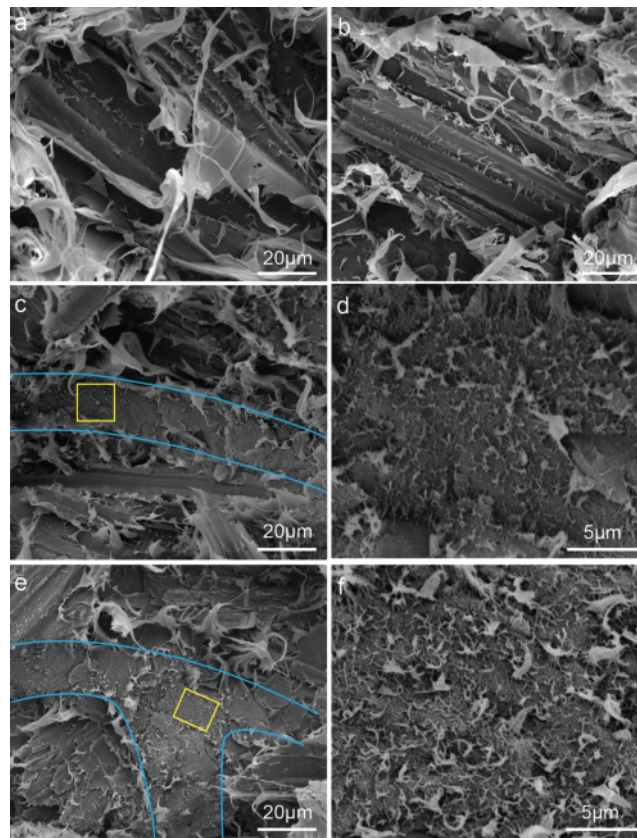


**Figure 4:** SEM micrographs of the flexural-fractured section of the WPC control panel (a,  $\times 1000$ ), WPC panel with fire retardant modified wood flour (b,  $\times 1000$ ), WPC panel with nSiO<sub>2</sub> network (c,  $\times 1000$ ; d  $\times 5000$ ), and WPC panel with nSiO<sub>2</sub> network and fire retardant modified wood flour (e,  $\times 1000$ ; f,  $\times 5000$ ). Yellow rectangles in (c) and (e) demonstrate the region shown in (d) and (f), respectively

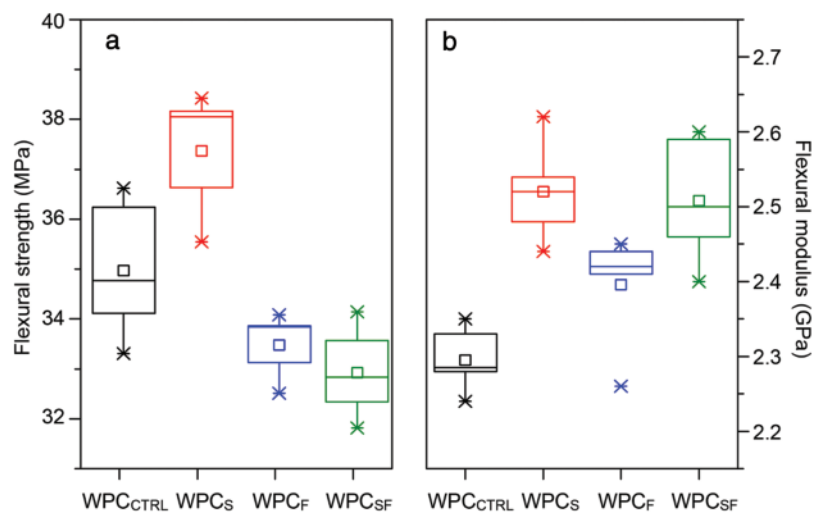


**Figure 5:** Flexural strength (a) and flexural modulus (b) of the WPC. (The abbreviations in the figure are the same with Tab. 1)

The flexural modulus of WPC<sub>S</sub> was 9.1% higher than that of the WPC<sub>CTRL</sub> due to the formation of a rigid nSiO<sub>2</sub> network (Fig. 5b). Unlike flexural strength, the flexural modulus of WPC<sub>F</sub> was higher than that of WPC<sub>CTRL</sub>. This was attributed to the positive effect of the rigid fire-retardant particles (DOT and GUP) on the modulus, which compensated for the negative effect of the weak interfacial effect between the modified-WF and HDPE [20]. The flexural modulus of WPC<sub>SF</sub> was higher than that of WPC<sub>F</sub>, which may have resulted from the combined action of rigid fire retardant particles and nSiO<sub>2</sub> network.

### 3.3 Creep and Relaxation Analysis

The creep resistances of the four WPC panels followed the order: WPC<sub>CTRL</sub> < WPC<sub>F</sub> < WPC<sub>SF</sub> < WPC<sub>S</sub> (Fig. 6a). The creep strain of WPC<sub>S</sub> (0.047%) was significantly lower than that of WPC<sub>CTRL</sub> (0.071%) after applying an external force for 45 min. This was attributed to the formation of a rigid nSiO<sub>2</sub> network in WPC<sub>S</sub>, which served as a rigid support that transmitted stress and provided deformation resistance. Compared with WPC<sub>CTRL</sub>, the lower creep strain of WPC<sub>F</sub> arose due to the introduction of the rigid fire retardant [1]. The creep strain of WPC<sub>SF</sub> was slightly higher than that of WPC<sub>S</sub>, possibly because the viscous substance wrapping the nSiO<sub>2</sub> reduced the rigidity of the nSiO<sub>2</sub> network in WPC<sub>SF</sub>. Similar to the improved creep resistance, the relaxation moduli of WPC<sub>S</sub>, WPC<sub>F</sub>, and WPC<sub>SF</sub> were higher than that of WPC<sub>CTRL</sub> (Fig. 6b). The relaxation modulus of WPC<sub>S</sub> was 21.3% higher than that of WPC<sub>CTRL</sub>, indicating that the introduction of a rigid nSiO<sub>2</sub> network effectively resisted the deformation of WPC caused by the constant external force.

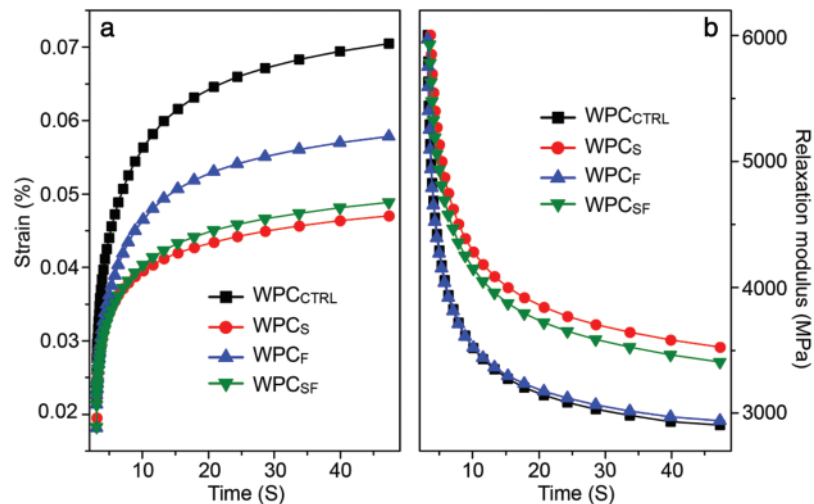


**Figure 6:** Creep strain (a) and relaxation modulus (b) of the WPC. (The abbreviations in the figure are the same with Tab. 1)

### 3.4 Thermal Expansion Behavior

The thermal expansion rates of WPC<sub>S</sub>, WPC<sub>F</sub>, and WPC<sub>SF</sub> were lower than that of WPC<sub>CTRL</sub> and ranged from -40 to 90°C (Fig. 7a). This was due to the presence of a rigid nSiO<sub>2</sub> network and fire retardant which were inherently not prone to thermal expansion [21]. The WPC<sub>SF</sub> showed the lowest thermal expansion rate over the test temperature range compared with the other WPC panels due to its higher nSiO<sub>2</sub> content. The thermal expansion rates of WPC<sub>SF</sub>, WPC<sub>F</sub>, WPC<sub>S</sub>, and WPC<sub>CTRL</sub> at 90°C were 19.9%, 24.3%, 24.2%, and 28.0%, respectively. The linear coefficient of thermal expansion (LCTE) increased with temperature, and a higher increment was observed after 50°C (Fig. 7b). This was because the thermal motion of HDPE increased with the temperature, causing an increase in the macroscopic volume of WPC [22]. It

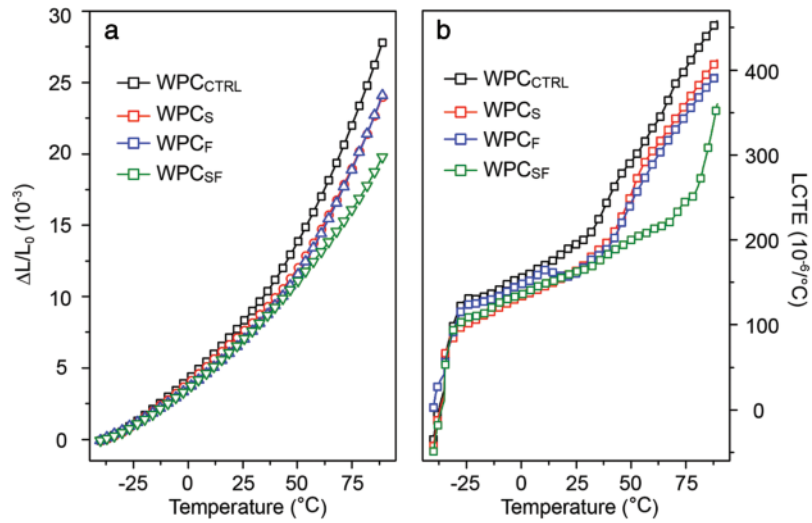


**Figure 7:** Thermal expansion rate (a) and linear coefficient of thermal expansion (b) of the WPC. (The abbreviations in the figure are the same with Tab. 1)

was found that the LCTE of WPC<sub>SF</sub> was significantly lower than that of WPC<sub>CTRL</sub>, suggesting that the wider rigid nSiO<sub>2</sub> network region effectively reduced the thermal expansion.

### 3.5 Combustion Characteristics

The WPC<sub>CTRL</sub> was burned to ashes (Fig. 8a). The white residual material on the surface of WPC<sub>S</sub> was nSiO<sub>2</sub>, and the bottom was mainly carbonized wood flour (Fig. 8b). The cracks produced on the WPC<sub>S</sub>

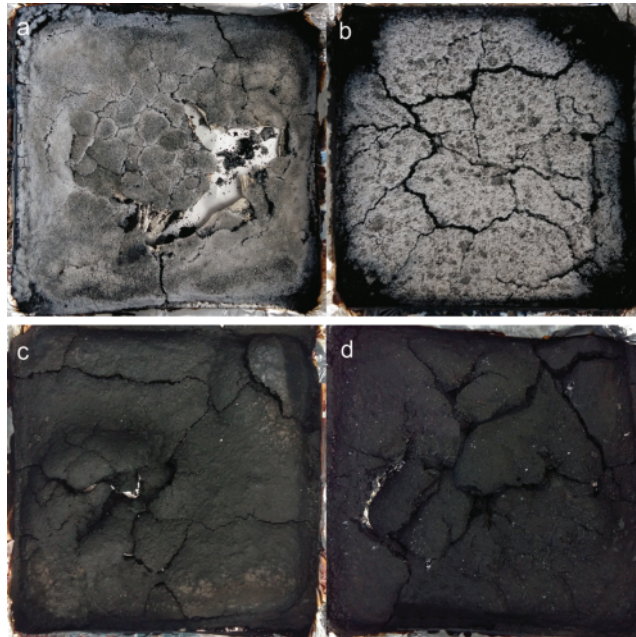


**Figure 8:** Digital photographs of the residues of four kinds of WPC after cone test: WPC control panel (a), WPC panel with nSiO<sub>2</sub> network (b), WPC panel with fire retardant modified wood flour (c), and WPC panel with nSiO<sub>2</sub> network and fire retardant modified wood flour (d)

residuals were caused by the gas impact, which was responsible for the higher smoke release of WPC<sub>S</sub> after 300 s. The residuals of WPC<sub>F</sub> also exhibited cracks (Fig. 8c). The combustion residuals of WPC<sub>SF</sub> were thicker than those of WPC<sub>F</sub> because the wider nSiO<sub>2</sub> network region hindered the gas release and the gas impulse caused the expansion of the residuals [4] (Fig. 8d). The physical integrity of the WPC<sub>F</sub> and WPC<sub>SF</sub> residues were poor, indicating a weak strength, which did not help reduce the heat and smoke release of WPC<sub>F</sub> and WPC<sub>SF</sub>. In contrast to WPC<sub>S</sub>, no nSiO<sub>2</sub> was deposited on the surface of the WPC<sub>SF</sub> residues, possibly because the APP and PPA produced by the decomposition of GUP reacted with nSiO<sub>2</sub> to form pyrophosphate silicon [13].

The WPC<sub>CTRL</sub> was burnt into short carbon fragments (Fig. 9a). Compared with WPC<sub>CTRL</sub>, the EDS results indicated the formation of an nSiO<sub>2</sub> crust on the residuals surface of WPC<sub>S</sub> (Fig. 9b) and a complete carbon skeleton of WF on the bottom of the residuals (not shown). The residuals of WPC<sub>F</sub> were dense (Fig. 9c), and their surfaces were coated by lamellar sodium octabonate (Fig. 9d). P and N were detected on the WPC<sub>F</sub> residuals by EDS (Fig. 9d), indicating that the degradation products of GUP, such as PPA, also remained on the surface of the residuals. Similar to WPC<sub>F</sub>, compact residuals were observed for WPC<sub>SF</sub> (Fig. 9e). Its surface was coated by a layer of a glassy substance containing Na, P, N, and Si (Fig. 9f), which indicated that this film may be composed of sodium octabonate, polyphosphoric acid, pyrophosphate silicon, and unreacted nSiO<sub>2</sub>.

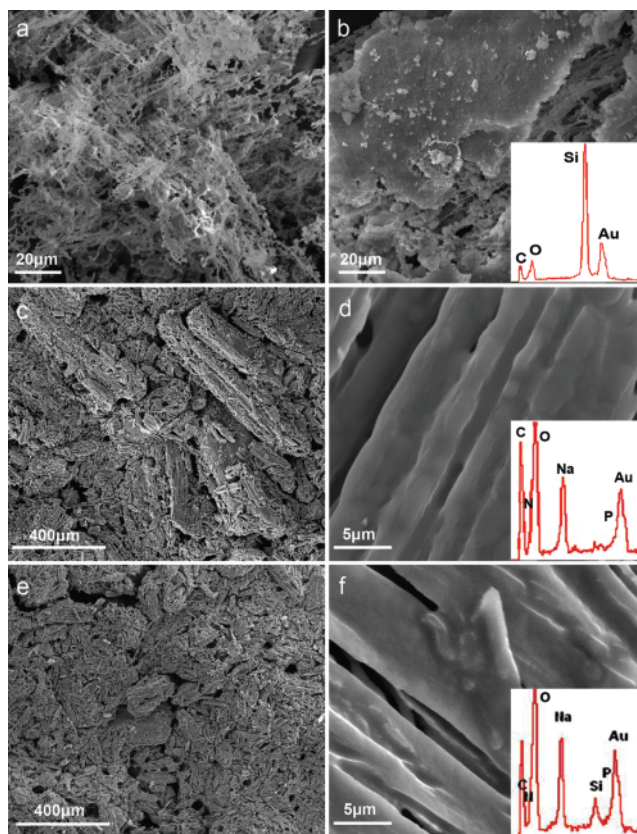


**Figure 9:** SEM of the WPC residual: the WPC<sub>CTRL</sub> (a,  $\times 1000$ ), the surface of WPC<sub>S</sub> (b,  $\times 1000$ ), the surface of WPC<sub>F</sub> (c,  $\times 100$ ; d,  $\times 5000$ ), the surface of WPC<sub>SF</sub> (e,  $\times 100$ ; f,  $\times 5000$ ), the line drawings in the lower right corner of figure (b), (d), and (f) are from EDS. (The abbreviations are the same with Tab. 1)

Compared with  $WPC_{CTRL}$ , the HRR of  $WPC_S$  decreased slightly before 300 s during combustion (Fig. 10a) because the  $nSiO_2$  network exerted physical shielding and catalytic charring effects [23]. However, the  $nSiO_2$  loading (0.55%) was insufficient to significantly decrease the HRR of  $WPC_S$ . After 300 s of combustion, the HRR of  $WPC_S$  was higher than that of  $WPC_{CTRL}$  (Fig. 10a) due to the formation of a large number of cracks on the surface of the residuals (Fig. 8b). These cracks provided channels for heat and combustible gases to penetrate, increasing the HRR [24]. The HRR and THR of  $WPC_F$  were lower than those of  $WPC_{CTRL}$  (Figs. 10a and 10b). The reasons for the reduction may be as follows: (1) the thermal decomposition reactions of the fire retardant (GUP and DOT) could absorb heat from the fire source. The small molecular gasses ( $H_2O$ ,  $NH_3$ , and  $CO_2$ ) produced by the decomposition of GUP and DOT could reduce the  $O_2$  concentration, which decreased oxidative pyrolysis [25]; (2) the glassy sodium borate that was produced from the degradation of DOT coated the residuals and provided physical protection [26]; (3) the decomposition products of GUP may have catalyzed the charring of WF [20]. Compared with  $WPC_F$ ,  $WPC_{SF}$  showed a slightly lower HRR and THR, which may have been due to the synergistic effect of the  $nSiO_2$  network and fire retardants (DOT and GUP).

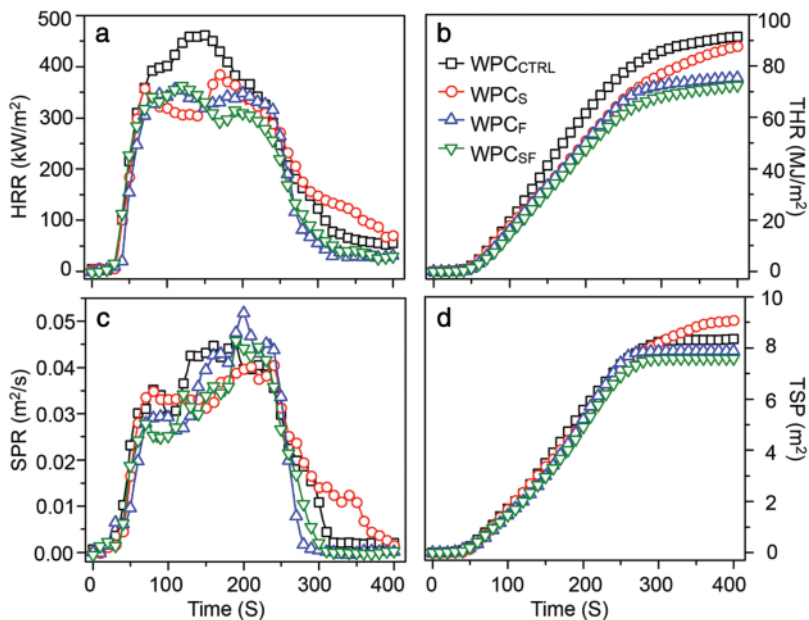


**Figure 10:** Heat release rate (HRR) (a), total heat release (THR) (b), smoke production rate (SPR) (c), and total smoke production (TSP) (d) of the WPC. (The abbreviations in the figure are the same with Tab. 1)

The SPR and TSP of  $WPC_S$  were higher after 300 s compared with those of  $WPC_{CTRL}$  (Figs. 10c and 10d). These increased values were due to the production of cracks in the residues during the later stage of combustion, which resulted in the combustion of the bottom substances and an increased smoke release [24]. As for  $WPC_F$ , an instantaneous increase in SPR was observed at 200 s. This may be due to the release of the bottom substances due to the local collapse of the residuals (Fig. 8c). The SPR and TSP of  $WPC_{SF}$  were lower than those of  $WPC_{CTRL}$ , although cracking occurred in the  $WPC_{SF}$  residuals (Fig. 8d). The shielding effect of the glassy sodium borate on the bottom substances and the release of  $H_2O$ ,  $NH_3$ , and  $CO_2$  during combustion reduced the combustion power, which decreased the smoke release of  $WPC_{SF}$ .

The combustion reactions are shown in Fig. 11. The silanol groups on the  $nSiO_2$  surface acted as active catalytic sites for Brønsted acids that catalyzed the carbonization of WF in  $WPC_S$  and  $WPC_{SF}$  by removing H

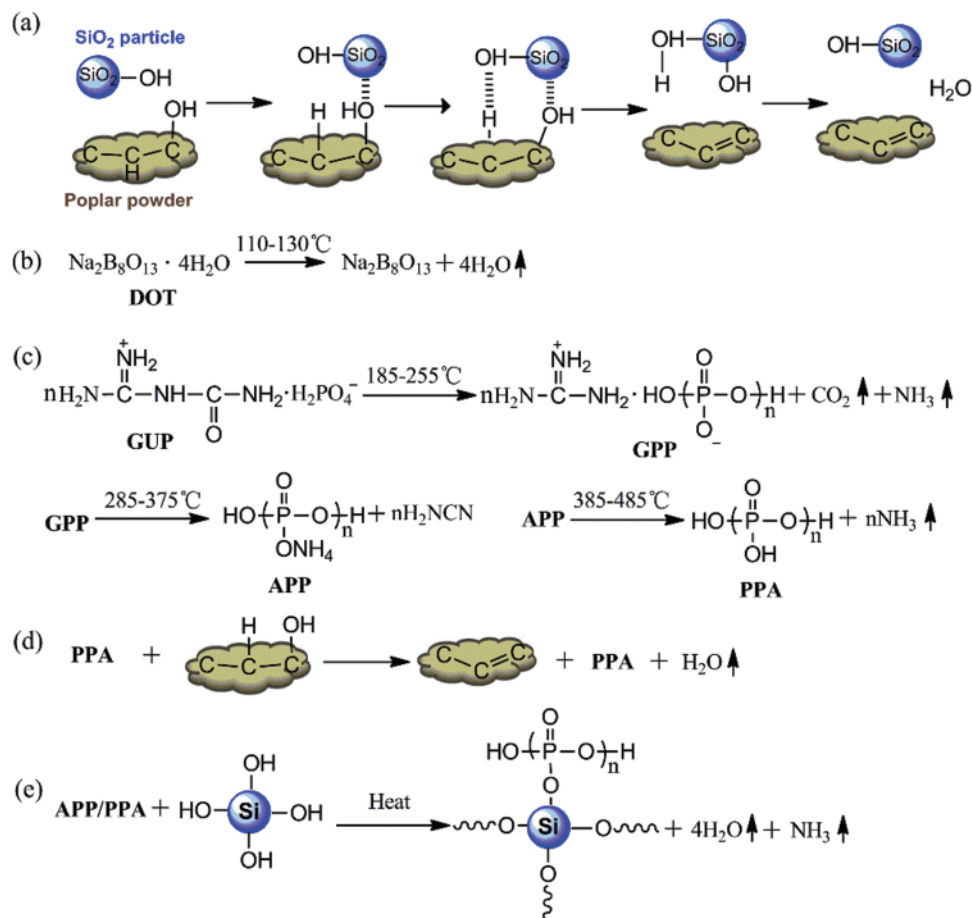


**Figure 11:** Possible reactions during combustion

and O (Fig. 11a). The formation of a carbonized layer protected the substrate from fire and heat, which decreased the heat release [27]. The DOT in WPC<sub>F</sub> and WPC<sub>SF</sub> decomposed into non-combustible sodium borate and water at 130°C. The sodium borate acted as a barrier, and the water could absorb heat as it evaporated, which both helped reduce the burning rate [28] (Fig. 11b). The GUP decomposed into CO<sub>2</sub>, NH<sub>3</sub>, and condensed guanidine phosphate (GPP) at temperatures higher than 185°C. The produced GPP further decomposed into ammonium polyphosphate (APP) above 285°C, and the APP decomposed into polyphosphate acid (PPA) and NH<sub>3</sub> above 380°C [29]. The APP and PPA then catalyzed the carbonization of WF by removing H and O [30] (Figs. 11c and 11d), and the formation of a stable carbon layer played a shielding effect to isolate the heat and O<sub>2</sub>. The APP or PPA generated during combustion reacted with the nSiO<sub>2</sub> in WPC<sub>SF</sub> to produce pyrophosphate silicon, H<sub>2</sub>O, and NH<sub>3</sub>, which could absorb heat and dilute O<sub>2</sub> (Fig. 11e) [13].

The mass retention of WPC<sub>S</sub> was similar to that of WPC<sub>CTRL</sub> (7.2%) after burning for 400 s due to the extremely low nSiO<sub>2</sub> loading in WPC<sub>S</sub> (Fig. 12). The mass retention of WPC<sub>F</sub> and WPC<sub>SF</sub> was obviously higher than that of WPC<sub>CTRL</sub> due to the formation of stable carbon layers. The mass-loss rates (the slope of the curve) of WPC<sub>S</sub>, WPC<sub>F</sub>, and WPC<sub>SF</sub> were lower than WPC<sub>CTRL</sub>, which indicated that the introduction of an nSiO<sub>2</sub> network and fire retardant reduced the burning rate of WPC.

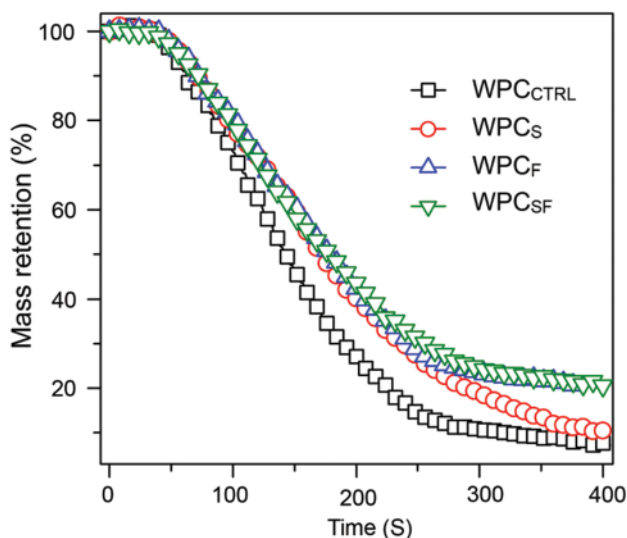


**Figure 12:** The mass retention of the WPC during combustion. (The abbreviations in the figure are the same with Tab. 1)

#### 4 Conclusions

In this study, a facile approach was used to fabricate WPC with a continuous honeycomb-like nano-SiO<sub>2</sub> network (WPC<sub>S</sub>). The rigid nano-SiO<sub>2</sub> network improved the strength and dimensional stability of WPCs at a considerably low nano-SiO<sub>2</sub> content (0.55 wt.%) compared with WPC<sub>CTRL</sub>. When the WF was modified with fire retardants (DOT and GUP), the flexural modulus and creep resistance of the network-structured WPC (WPC<sub>SF</sub>) also increased compared with WPC<sub>CTRL</sub>. WPC<sub>SF</sub> showed the lowest thermal expansion rate and LCTE, and its flexural strength only decreased by 5.5% compared with that of WPC<sub>CTRL</sub>. Additionally, WPC<sub>SF</sub> showed an improved fire retardancy compared with WPC<sub>CTRL</sub>. The results presented here demonstrated that an efficient and facile procedure could be used to produce WPC with desired functions through the formation of continuous honeycomb-like nanoparticle networks.

**Funding Statement:** This work was supported by the National Key Research and Development Program of China (Nos. 2019YFD1101204 and 2019YFD1101203), the National Natural Science Foundation of China (Nos. 31870547 and 31901251), the Project funded by China Postdoctoral Science Foundation (No. 2019M652919), the Research and Development Program in Key Areas of Guangdong Province (No. 2020B020216002), the Project of Guangzhou Municipal Key Laboratory of Woody Biomass Functional New Materials (No. 201905010005), and the Project of Key Disciplines of Forestry Engineering of Bureau of Education of Guangzhou Municipality.

**Conflicts of Interest:** The authors declare that they have no conflicts of interest to report regarding the present study.

#### References

1. Hao, X., Yi, X., Sun, L., Tu, D., Wang, Q. et al. (2019). Mechanical properties, creep resistance, and dimensional stability of core/shell structured wood flour/polyethylene composites with highly filled core layer. *Construction and Building Materials*, 226, 879–887. DOI 10.1016/j.conbuildmat.2019.07.329.
2. Meenakshi, C. M., Krishnamoorthy, A. (2019). Study on the effect of surface modification on the mechanical and thermal behaviour of flax, sisal and glass fiber-reinforced epoxy hybrid composites. *Journal of Renewable Materials*, 7(2), 153–169. DOI 10.32604/jrm.2019.00046.

3. Tazi, M., Erchiqui, F., Godard, F., Kaddami, H. (2014). Evaluation of mechanical properties and durability performance of HDPE-wood composites. *Journal of Renewable Materials*, 2(4), 258–263. DOI 10.7569/JRM.2014.634120.
4. Zhou, H., Xiao, Z., Wang, Y., Hao, X., Xie, Y. et al. (2020). Conductive and fire-retardant wood/polyethylene composites based on a continuous honeycomb-like nanoscale carbon black network. *Construction and Building Materials*, 233, 117369–117377. DOI 10.1016/j.conbuildmat.2019.117369.
5. Guan, Y. H., Huang, J. Q., Yang, J. C., Shao, Z. B., Wang, Y. Z. (2015). An effective way to fire-retard biocomposite with ethanolamine modified ammonium polyphosphate and its fire retardant mechanisms. *Industrial & Engineering Chemistry Research*, 54(13), 3524–3531. DOI 10.1021/acs.iecr.5b00123.
6. Hao, X., Zhou, H., Wang, Q., Wang, H., Song, Y. et al. (2018). Reinforcement of wood flour/HDPE composite with a copolyester of p-hydroxy benzoic acid and 2-hydroxy-6-naphthoic acid. *Journal of Applied Polymer Science*, 47338(15), 1–8. DOI 10.1002/app.47338.
7. Subrahmanian, V., Albert, N. E. M. (2019). Studies on physical chemistry of rubber-rice husk ash composites. *Journal of Renewable Materials*, 7(2), 171–192. DOI 10.32604/jrm.2019.00090.
8. Gao, H., Xie, Y., Ou, R., Wang, Q. (2012). Grafting effects of polypropylene/polyethylene blends with maleic anhydride on the properties of the resulting wood-plastic composites. *Composites Part A: Applied Science and Manufacturing*, 43(1), 150–157. DOI 10.1016/j.compositesa.2011.10.001.
9. Lee, S. Y., Yang, H. S., Kim, H. J., Jeong, C. S., Lim, B. S. et al. (2004). Creep behavior and manufacturing parameters of wood flour filled polypropylene composites. *Composite Structures*, 65(3–4), 459–469. DOI 10.1016/j.compstruct.2003.12.007.
10. Yadav, S. M., Yusoh, K. B. (2018). Subsurface mechanical properties and subsurface creep behaviour of modified nanoclay-based wood-plastic composites studied by nanoindentation. *Polymer Bulletin*, 76(5), 2179–2196. DOI 10.1007/s00289-018-2497-5.
11. Liu, R., Luo, S., Cao, J., Peng, Y. (2013). Characterization of organo-montmorillonite (OMMT) modified wood flour and properties of its composites with poly(lactic acid). *Composites Part A: Applied Science and Manufacturing*, 51, 33–42. DOI 10.1016/j.compositesa.2013.03.019.
12. Siengchin, S., Dangtungee, R. (2014). Polyethylene and polypropylene hybrid composites based on nano silicon dioxide and different flax structures. *Journal of Thermoplastic Composite Materials*, 27(10), 1428–1447. DOI 10.1177/0892705714526916.
13. Pan, M., Mei, C., Du, J., Li, G. (2014). Synergistic effect of nano silicon dioxide and ammonium polyphosphate on flame retardancy of wood fiber-polyethylene composites. *Composites Part A: Applied Science and Manufacturing*, 66, 128–134. DOI 10.1016/j.compositesa.2014.07.016.
14. Zhou, H., Hao, X., Wang, H., Wang, X. Y., Liu, T. et al. (2018). The reinforcement efficacy of nano- and microscale silica for extruded wood flour/HDPE composites: the effects of dispersion patterns and interfacial modification. *Journal of Materials Science*, 53(3), 1899–1910. DOI 10.1007/s10853-017-1650-0.
15. Pan, M. Z., Lian, H. L., Mei, C. T. (2012). Flammability of nano silicon dioxide-wood fiber-polyethylene composites. *Journal of Composite Materials*, 47(12), 1471–1478. DOI 10.1177/0021998312448499.
16. Jiang, L., Wolcott, M. P., Zhang, J., Englund, K. (2007). Flexural Properties of surface reinforced wood/plastic deck board. *Polymer Engineering & Science*, 47(3), 281–288. DOI 10.1002/pen.20705.
17. Potts, J. R., Shankar, O., Du, L., Ruoff, R. S. (2012). Processing-morphology-property relationships and composite theory analysis of reduced graphene oxide/natural rubber nanocomposites. *Macromolecules*, 45(15), 6045–6055. DOI 10.1021/ma300706k.
18. Donmez, C. A., Mengeloğlu, F., Karakus, K. (2015). Effect of boric acid and borax on mechanical, fire and thermal properties of wood flour filled high density polyethylene composites. *Measurement*, 60, 6–12. DOI 10.1016/j.measurement.2014.09.078.
19. Baysal, E., Yalinkilic, M. K., Altinok, M., Sonmez, A., Peker, H. et al. (2007). Some physical, biological, mechanical, and fire properties of wood polymer composite (WPC) pretreated with boric acid and borax mixture. *Construction and Building Materials*, 21(9), 1879–1885. DOI 10.1016/j.conbuildmat.2006.05.026.

20. Ayrlimis, N., Akbulut, T., Dundar, T., Mengelolu, F., Buyuksari, U. et al. (2012). Effect of boron and phosphate compounds on physical, mechanical, and fire properties of wood-polypropylene composites. *Construction and Building Materials*, 33, 63–69. DOI 10.1016/j.conbuildmat.2012.01.013.
21. Suzuki, N., Kiba, S., Yamauchi, Y. (2011). Bimodal filler system consisting of mesoporous silica particles and silica nanoparticles toward efficient suppression of thermal expansion in silica/epoxy composites. *Journal of Materials Chemistry*, 21(38), 14941–14947. DOI 10.1039/c1jm12405f.
22. Rao, Y. Q., Blanton, T. N. (2008). Polymer nanocomposites with a low thermal expansion coefficient. *Macromolecules*, 41(3), 935–941. DOI 10.1021/ma7020216.
23. Kashiwagi, T., Gilman, J. W., Butler, K. M., Harris, R. H., Asano, A. (2000). Fire retardant mechanism of silica gel/silica. *Fire & Materials*, 24, 277–289. DOI 10.1002/1099-1018(200011/12)24:63.O.CO;2-A.
24. Zhao, Q., Zhang, B., Quan, H., Yam, R. C. M., Yuen, R. K. K. et al. (2009). Fire retardancy of rice husk-filled high-density polyethylene ecocomposites. *Composites Science and Technology*, 69(15–16), 2675–2681. DOI 10.1016/j.compscitech.2009.08.009.
25. Winandy, J. E., Wang, Q., White, R. H. (2008). Fire-retardant-treated strandboard: properties and fire performance. *Wood and Fiber Science*, 40(1), 62–71. DOI 10.1177/0040517507082635.
26. Wu, G. F., Xu, M. (2014). Effects of boron compounds on the mechanical and fire properties of wood-chitosan and high-density polyethylene composites. *BioResources*, 9, 4173–4193.
27. Tsutsumi, K., Kurata, N., Takata, E., Furuichi, K., Nagano, M. et al. (2014). Silicon semiconductor-assisted Brønsted acid-catalyzed dehydration: highly selective synthesis of 5-hydroxymethylfurfural from fructose under visible light irradiation. *Applied Catalysis B: Environmental*, 147, 1009–1014. DOI 10.1016/j.apcatb.2013.10.032.
28. Wang, Q., Li, J., Winandy, J. (2004). Chemical mechanism of fire retardance of boric acid on wood. *Wood Science and Technology*, 38(5), 375–389. DOI 10.1007/s00226-004-0246-4.
29. Li, B., Zhang, X., Su, R. (2002). An investigation of thermal degradation and charring of larch lignin in the condensed phase: the effects of boric acid, guanyl urea phosphate, ammonium dihydrogen phosphate and ammonium polyphosphate. *Polymer Degradation and Stability*, 75(1), 35–44. DOI 10.1016/S0141-3910(01)00202-6.
30. Samyn, F., Bourbigot, S., Duquesne, S., Delobel, R. (2007). Effect of zinc borate on the thermal degradation of ammonium polyphosphate. *Thermochimica Acta*, 456(2), 134–144. DOI 10.1016/j.tca.2007.02.006.